Superconductors: The Conductivity of Focused Ion Beam Carbon Depositions and the Josephson junction of $(TMTSF)_2ClO_4$

An Honors Thesis by

Liam Norris

0.0 Abstract

This paper details two projects relating to superconductivity carried out at Boston College over the summers of 2008 and 2009. In one project, I investigated the conductivity of focused ion beam (FIB) carbon depositions. I raised a FIB carbon deposition's oxygen concentration to 25% oxygen by exposing it to oxygen plasma generated by a plasma microwave system followed by the heat of a tube furnace. The oxygen doped FIB carbon deposition did not exhibit superconductivity. The second project was an attempt to create a Josephson Junction using the organic superconductor $(TMTSF)_2ClO_4$ to characterize the spin and angular momentum of the electrons involved in its Cooper pairing mechanism. I successfully cleaved the organic superconductor $(TMTSF)_2ClO_4$ along its most conductive axis but three attempts to form a Josephson junction along the cleaved plane were unsuccessful.

1.0 Introduction

Superconductors have seen several useful applications in engineering and the sciences. Superconducting quantum interference devices (a.k.a. "SQUIDs") make extremely accurate measurements of magnetic fields (N. Butch et al., 2008). The creation of high temperature superconductors could make the construction of maglev trains more feasible. Superconductors are also widely used in magnetic resonance imaging (Thornton and Rex, 1993, p. 355), which have made significant advances in the diagnostic capabilities of the medical field.

The two projects that I carried out at Boston College over the summers of 2008 and 2009 were closely related to the pursuit of understanding superconductivity. In the summer of 2009, I was interested in seeing if amorphous depositions of carbon formed with a focused ion beam (FIB) could become superconducting. In the summer of 2008, I was interested in characterizing the mechanism of superconductivity in the organic crystal $(TMTSF)_2ClO_4$. To summarize the similarities and differences between the two projects: in the first, I was interested in creating a new superconductor while, in the second, I was investigating the properties of a known superconductor.

The investigation of conductivity in FIB carbon depositions was motivated by the discovery of a superconducting sample with a critical temperature of 7 K in November of 2008 (Dhakal et al., 2009). Superconductivity in FIB carbon depositions had not been observed previously. The sample was created using the FIB in a normal fashion but it was observed through energy dispersive x-ray spectrometry that it had an unusual concentration of oxygen and gallium (37.5% ± 3.5% and 26.1% ± 2.6%, respectively). In an effort to ultimately reproduce the superconductivity in a FIB carbon deposition, I experimented with several methods of raising the concentration of oxygen in samples.

The capacity to make FIB carbon depositions superconducting would enable laboratories around the world to explore the properties of superconductors with unusual geometries.

The goal of the second project was to characterize the superconductivity in the organic crystal $(TMTSF)_2ClO_4$. "TMTSF" stands for "**T**etra**M**ethyl**T**etra**S**elena**F**ulvalene" and is more accurately described as Di(2,3,6,7-tetramethyl-1,4,5,8-tetraselenafulvalenium). Superconductivity occurs through the pairing of electrons, which can take on angular momentum with an azimuthal quantum number l of 0, 1, or 2, corresponding to a spin configuration of singlet, triplet or singlet, respectively. While the majority of superconductors have paired electrons in the singlet state, a handful of experiments suggest that, the organic superconductor $(TMTSF)_2PF_6$ is a material with triplet superconductivity (I. Lee et al. 1997, I. Lee et al., 2000 and I. Lee et al., 2002—to name a few). Since $(TMTSF)_2ClO_4$ and $(TMTSF)_2PF_6$ share very similar crystal structures, $(TMTSF)_2ClO_4$ has also been investigated to see if it also exhibits exotic superconductivity. Although two experiments (H. Ha et al., 2003 and S. Belin and K. Behnia, 1997) suggest triplet superconductivity in $(TMTSF)_2ClO_4$, there isn't as much experiment evidence for it as there is in $(TMTSF)_2PF_6$ (W. Zhang and C. Sa de Melo, 2007). By arranging two $(TMTSF)_2ClO_4$ crystals so that they are separated by a very short (0.1 nm) gap in an arrangement referred to as a "Josephson junction," I could take measurements that could determine triplet or singlet superconductivity in the organic crystal (Vaccarella et al., 2003). Such an experiment would take the scientific community one step closer to characterizing the superconductivity in the $(TMTSF)_2ClO_4$.

In the rest of the paper, I present the projects in order of increasing depth and complexity of background information. Since superconductivity in FIB carbon depositions is a new phenomenon that has not been studied in great detail, there is less background information to cover. For this reason, the project carried out in the summer of 2009 will be presented first in Section 3. On the other hand, a thorough description of the theory behind triplet superconductivity and how it may be measured is considerably more involved. Hence the details of the project carried out in the summer of 2008 will be discussed in Section 4. But before discussing the individual projects, I will first give a brief introduction into the distinguishing properties of superconductors in Section 2.

2.0 Superconductivity

In Section 2.1, I will provide a description of the experimentally observed properties of superconductors. The majority of these properties will be explained by a brief intorduction into the theory of superconductivity proposed by Bardeen, Cooper, and Schrieffer 1958 in Section 2.2.

2.1 Experimental Properties of Superconductors

A material is identified as a superconductor if it exhibits zero resistance and can shield out magnetic fields. These properties are exhibited only at fairly low temperatures and in fairly weak magnetic fields. The exact threshold or "critical" temperature, T_c, and magnetic field, B_c, are specific to a given material. The exact critical magnetic field and critical temperature are more or less proportional to one another, with B_c ranging from 10^{-5} T up to 10^{-1} T for materials with critical temperatures below 1 mK to about 10 K, respectively. To give an example, a material can be made to transition between "normal" and "superconducting" phases by first cooling the material below its critical temperature.

Then a transition back to the "normal" phase can be achieved by applying a magnetic field stronger than B_c. For most superconductors, the critical temperature is on the order of Kelvin and so superconductivity is a phenomenon that is rarely seen outside of laboratories.

Newcomers to the field tend to be skeptical about whether the resistance actually drops below zero or if it is simply a very small number. While it is impossible to completely rule out the possibility of *some* resistance in a superconductor, very accurate measurements have been taken that show that it may be undetectable. Consider, for example, that the current induced in a metallic ring in a fluctuating magnetic field will decay over time, t, as

$$I(t) = I(0)\exp(-\frac{R}{L}t) \qquad \textit{Equation 1}$$

where the resistance of the ring and its self-inductance are represented by R and L, respectively. Electronic devices can measure $I(t)$ very accurately by observing the torque exerted by the metallic ring upon a concentric one if the second carries a known current. Such a measurement was performed with a superconducting ring instead of a metallic one for two and a half years. The absence of any detectable decay in the current placed an upper limit of 10^{-23} Ω-m (Lynton, 1962, p. 3). With this evidence, whether there is actually zero resistance or an undetectable resistance is simply a question of semantics.

In addition to being a perfect conductor, superconductors exhibit interesting magnetic properties (Griffiths, 1999, p. 335). The magnetic field within the interior of a superconductor is always zero. This perfect diamagnetism, as illustrated in Figure 1, is called the "Meissner Effect" (Abrikosov, 1988, p. 316). Figure 1 compares the internal magnetic field in a normal metal with that of a superconductor.

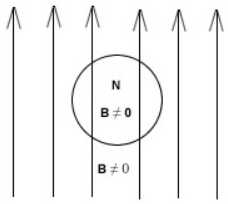

Figure 1a

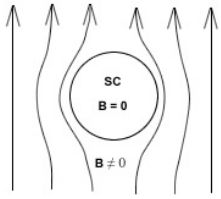

Figure 1b

In Figure 1a, a normal metal sphere, indicated by an "N," allows the penetration of an external magnetic field, represented by upward pointing arrows. In Figure 1b, a superconducting sphere, indicated by an "SC," expels the same applied external field, which is still represented by upward pointing arrows. The magnetic field deep within the interior of the superconductor is completely zero.

The Meissner effect occurs regardless of whether the external magnetic field is applied before or after the normal metal transitions into the superconducting phase. This is a feature that distinguishes it from a perfect conductor, which would "lock-in," or retain, any magnetic flux it experiences during its transition from a normal metal to a superconductor. Since the magnetic field within the interior of the superconductor is zero and currents produce magnetic fields, the current that runs through a superconductor exists only within a surface layer. This is analogous to how a charge resides only on the surface of a regular conductor (Griffiths, 1999, p. 97)

Along with that surface layer of current is a layer of field penetration. The depth of this penetration decays exponentially with the distance, a, into the superconductor as

$$B(a) = B_0 e^{-\frac{a}{\delta}} \qquad \textit{Equation 2}$$

Where B_0 is the magnetic field immediately outside of the superconductor and δ is the penetration depth as described by

$$\delta = \sqrt{\frac{m}{\mu_0 n e^2}\left[1-\left(\frac{T}{T_c}\right)^4\right]^{-1}} \qquad \textit{Equation 3}$$

where μ_0 is the permittivity of free space, m is the mass of the electron, e is the charge of the electron, T is the temperature, T_c is the critical temperature of the superconductor, and n is the total effective number of free electrons per unit volume in the metal, which is usually 10^{29} m^{-3} (Hook and Hall, 1991, p. 288).

With respect to critical fields, there are two types of superconductors: Type I and Type II. Type I superconductors have a single critical field B_c, below which a superconductor will exhibit superconductivity and above which the superconductivity dies off. The critical field, B_c, has been experimentally determined as a function of the temperature and the material's critical temperature by a parabolic equation:

$$\frac{B_c}{B_0} = 1-\left(\frac{T}{T_c}\right)^2 \qquad \textit{Equation 4}$$

Where B_0 is the theoretical critical field at absolute zero. A plot of the critical field as a function of temperature is shown in Figure 2.

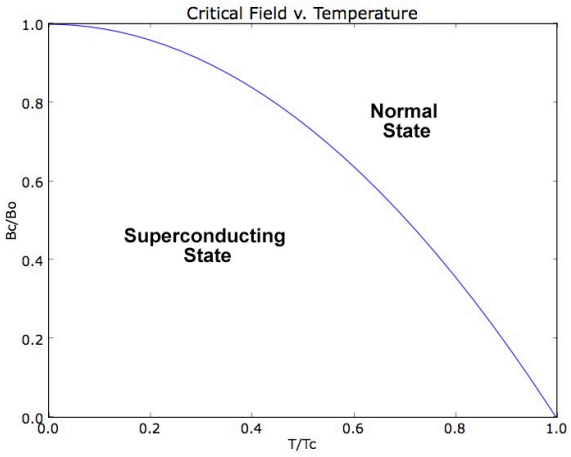

Figure 2

Critical field v. temperature of a conventional superconductor. At low temperatures relative to T_C, a greater magnetic field is necessary to kill the superconductivity within a material.

In a Type II superconductor, two critical fields, B_{c1} and B_{c2} exist. Below B_{c1}, superconductivity occurs normally and above B_{c2}, it does not occur. Between B_{c1} and B_{c2}, a mixture of superconductivity and normal conductivity occurs.

Another intrinsic property of superconductors is that the critical temperature of a superconductor varies with isotopic mass. Two samples of the same chemical

composition but of different atomic isotopes have different critical temperatures. In fact, a less abrupt superconducting transition occurs if the material is composed of a variety of isotopes. The critical temperature, T_c, of a superconductor varies with its molecular mass, M, as

$$M^{\alpha}T_c = cons. \qquad \textit{Equation 5}$$

Where α is measured experimentally for each element. This property of superconductors is referred to as the "Isotope Effect" and, more than any other property, suggests that the mechanism behind superconductivity is dependent upon the lattice structure of the superconductor.

2.2 Microscopic Theory of Superconductivity

The theory proposed by Bardeen, Cooper, and Shrieffer (BCS) that effectively explains most low temperature superconductivity states that it is caused by phonons mediating the pairing of electrons into so-called Cooper pairs (Abrikosov, 1988, p.334). These pairs have two interesting properties. First, the pair has integer spin and thus obeys Bose-Einstein statistics rather than Fermi-Dirac statistics and so multiple pairs can share the same composite wave function. Second, the paired electrons are immune to collisions that are not strong enough to break their pairing, much like how atomic electrons cannot be excited by photons of insufficient energy.

In low temperature, Type I Superconductors, the attractive interaction that forms the Cooper pair is due to the lattice of ions in the metal[1]. One electron, in its trajectory through the metal, exerts an attractive electric force upon the lattice of positively charged ions. The wave function that describes the position of the particle creates points of maximum probability that create distortions in the ion lattice such that positive densities of ions form. Another electron with opposite momentum will pass across this array of positive densities so that eventually its points of most probable position overlap with the original electron. Eventually, the electrons form a standing wave that represents the Cooper pair. These lattice distortions are quantifiable and are called "phonons." Cooper pairs are therefore mediated by phonons as illustrated in Figures 3a, 3b, and 3c.

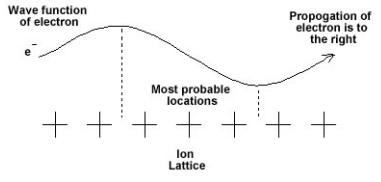

Figure 3a

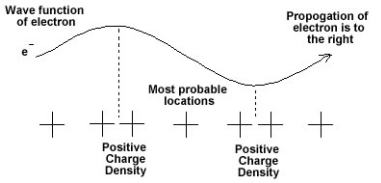

Figure 3b

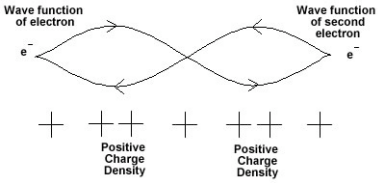

Figure 3c

In Figures 3a, 3b, and 3c, the seven plus signs represent positively charged ions in the atomic lattice of a superconductor. In Figures 3a and 3b, the wave function of the electron propagates to the right with points of maximum probability marked. The positive charges are attracted to these maximum probabilities and shift towards the higher concentration of negative charge in Figure 3b. Figure 3c shows how a second electron of momentum opposite to the first yields an overlapping wavefunction reinforced by the positive charge densities.

[1] This simplified explanation of the phonon interaction is a result of discussions with Eric Hill at the University of Redlands in 2010. Please encourage him to publish his theoretical descriptions of superconductivity.

This "attractive force" between two electrons causes the formation of the Cooper pair.

The Cooper pair formation lowers the energy so that the participating electrons prefer to remain "bound" to each other. At low enough temperatures, typical phonons, which have energy proportional to $k_B T$ (where k_B is Boltzman's constant T is the temperature of the superconductor), typical phonons are too weak to break this "bond." This energy "gap" is typically referred to as 2Δ, where Δ can be calculated and measured for specific materials. The energy gap, Δ, has a temperature dependence that can be described in Equation 6 (Abrikosov, 1988, p. 347):

$$\Delta(T) = 3.06 k_B T_c \sqrt{1 - \frac{T}{T_c}} \qquad \text{Equation 6}$$

A sketch of this temperature dependence is shown in Figure 4. Notice that BCS Theory accommodates for observations by letting the energy gap go to zero when the temperature is equal to the critical temperature. This suggests that no Cooper pairs are formed at the critical temperature and so the material should not exhibit superconductivity at or above that temperature.

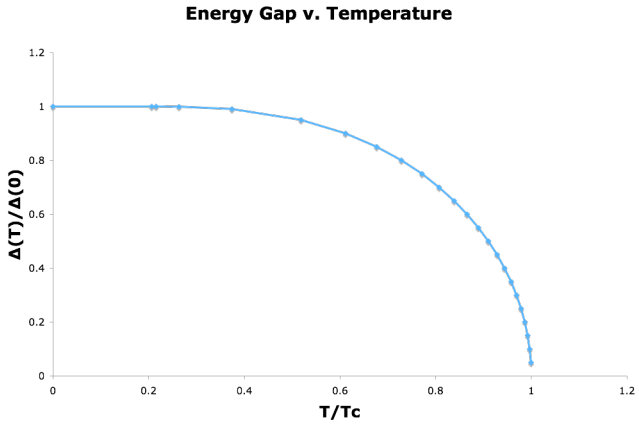

Figure 4

Energy gap temperature dependence. The important features are that the energy gap is appropriately zero at the critical temperature, which corresponds to an absence of Cooper pairs. The energy gap is greatest when all the electrons form Cooper pairs at absolute zero.

BCS Theory explains the existence of critical temperatures in superconductors thermodynamically. Cooper pair formation requires a cool ion lattice so that the ion's random thermal jiggling does not overwhelm the positive charge density presented by the pair of electrons. If the ion lattice is sufficiently heated, high energy phonons can knock electrons out of the potential well. The phonon interaction also explains the strong dependence of the critical temperature on the lattice mass as indicated in Equation 5.

The isotope effect can be explained by BCS theory. The energy of a phonon is similar to that of a photon, hence the similarity of nomenclature. But rather than propagate at the speed of light, phonons move only at the speed of sound in a material. When approximating the ion lattice as an array of springs with spring constants k

separated by a distance d, the speed of sound is $v_{sound} = d\sqrt{k/m}$. Taking the energy of the phonon to be proportional to $k_b T_c$, we have

$$E_{phonon} = \frac{hv}{\lambda} = \frac{h}{\lambda}\sqrt{\frac{k}{m}} \propto k_B T_c$$

$$\frac{h}{\lambda}\frac{\sqrt{k}}{k_B} = T_c\sqrt{m}$$

$$const. = T_c\sqrt{m}$$

which gives a rough sketch for the existence of the isotope effect.

The critical magnetic field is also explicable in terms of BCS Theory. In superconductors, the momenta of the electrons in a Cooper pair are opposite so that they can form standing waves. When placed in a magnetic field, the two electrons will therefore experience opposing magnetic forces due to the Lorentz force. At a sufficiently high magnetic field the magnetic forces on the two electrons will overcome the attractive phonon interaction and rip all the Cooper pairs in a material apart. Not surprisingly, critical field and critical temperature are roughly correlated. Robust superconductors can tolerate high temperatures and fields (~10 K, ~ 0.1 T) while more delicate ones can tolerate only low temperatures or fields (~1 mK, 10^{-5} T).

Last, but not least, the Meissner effect may also be understood in terms presented by BCS Theory. In the presence of a weak magnetic field (i.e., not stronger than B_c), an electron prefers to propagate in a circular path. Cooper pairing can only occur, however, if one electron moves with opposite momentum to the first. Hence a Cooper pair in a weak magnetic field consists of one electron moving as it normally would in a circular direction and another one moving *against* the Lorentz force in a circular path with opposite momentum. Since one electron is moving with the Lorentz force and one is moving against, the first is moving faster than the latter and so net current flows across along in a circular loop. This circular loop provides a magnetic shield to all of the electrons on the interior of the surface. The surface of the superconductor, left unshielded, thus experiences some magnetic field penetration due to a lack of shielding.

3.0 Exploring the Conductivity of Focused Ion Beam Depositions

The conductivity of elemental carbon is a fascinating subject because it can be an insulator in its diamond allotropic form or a conductor in its graphite form (Griffiths, 1999, p. 286). In 2008, Pashupati Dhakal unintentionally produced a superconducting oxygen-rich carbon sample by focused ion beam (FIB) controlled carbon deposition. For the summer of 2009, I worked to establish a process for reproducing this result. Dhakal measured a high oxygen and gallium concentrations in the sample, while FIB carbon depositions typically have no oxygen concentration but some gallium present. The goal of my research was to raise oxygen concentration in a FIB carbon deposition and see if this would lead to superconductivity. While Dhakal reported a 37.5 % oxygen concentration, I found that the oxygen concentration of FIB carbon deposition could be raised to be 25 % by exposing it to a combination of heat and oxygen plasma. Dhakal also reported that the sample began to transition to the superconducting state at 7 K. However, this increased oxygen concentration in my samples did not result in superconductivity at temperatures above 4.2 K.

In the following presentation of my results, I will first describe how the FIB carbon depositions were prepared for study in Section 3.1. Then I present the results of exposing the prepared depositions to plasma, heat, and a combination of heat and plasma in Sections 3.2, 3.3, and 3.4, respectively. The results of Sections 3.2-3.4 are then used then applied to Section 3.5, which details the preparation of a larger sample that was submerged into liquid helium in an attempt to achieve a transition to the superconducting state. I provide some concluding remarks in Section 3.6.

3.1 FIB Carbon Deposition Preparation

"Focused ion beam" is a term that refers to either a beam of ions or a device that produces such a beam. FIBs are used to locally alter material in the nanometer range and so are excellent nanofabrication tools. The FIB that I worked with, the JIB-4500 Multibeam SEM/FIB, could be used to cut, or "mill," at target areas or make amorphous depositions of tungsten or carbon. A schematic of a FIB is shown in Figure 5. The FIB consists of a heated liquid ion source that emits ions towards a "beam control," which is a series of lenses that manages the precise destinations of the ions emitted, similar to how an electron beam is aimed in the cathode ray tube of a television. The ion source for the JIB-4500 was liquid Gallium, which boils just above room temperature at ~30 ºC.

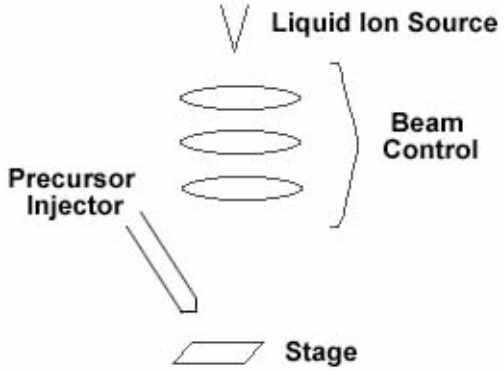

Figure 5

A schematic representation of a Focused Ion Beam. A series of lenses, referred to as the "Beam Control," direct the trajectory of ions emitted from the liquid ion source. The precursor gas phenanthrene, which is placed onto the stage by the "Precursor Injector," forms an amorphous carbon deposition when the emitted ions collide with it. (Utke, 2008)

The FIB creates a carbon deposition first by injecting the precursor gas, phenanthrene onto the stage. The FIB then launches a layer of gallium ions to a rectangular target area by moving its focus between spots, which are arranged in rows and columns across the target area. The time that the beam focuses on a single spot is referred to as the "dwell time" and the rate at which the ions hit the substrate is simply the "current." Once the spots in all the rows and columns have been targeted, a fresh injection of phenanthrene ($C_{14}H_{10}$) is supplied for a period of time referred to as the "interval." This process is repeated until a desired total charge density, called the "dose," is supplied by the charged Gallium ions. The beam number, or simply the "beam," is an index of the beam spot size, with larger numbers corresponding to larger beams. The

spots can overlap by setting the "Beam Overlap X/Y" to some fraction of unity, indicating an overlap equal to that fraction.

Unless otherwise noted, the word "sample" refers to a 4 micrometer x 10 micrometer FIB carbon deposition that was produced with the parameters listed in Table 1. Given a dose of 2 nC/μm^2, the samples were roughly 1 micrometer tall. The substrate for all samples was always silicon. I used an energy dispersive x-ray spectrometry system to determine the chemical composition of all the samples presented and I used a scanning electron microscope to capture the images presented in Figures 9a, 9b, 10, 11, and 12.

Parameter	**Value**
Dose	2 nC/μm^2
Dwell time	0.4 μs
Interval	1 ms
Beam	7
Beam Overlap X	0.5
Beam Overlap Y	0.5
Current	300 pA

Table 1

An oxygen concentration of only 1 % was present in all samples made by the FIB. Variation of the above parameters resulted in minimal variation in the concentration of oxygen in the sample. Variation included creating identical depositions but altering the dose to 4 nc/μm^2, the dwell time to 1 μs, the interval to 0 ms, 2 ms and 4 ms, adjusting the Fine-Z distance and the temperature control. The Fine-Z distance is the distance from the beam to the substrate. Submerging the substrate in water also did not affect the concentration of oxygen in the sample. These preliminary tests conclude that the source of oxygen in Dhakal's superconducting FIB carbon deposition to be truly mysterious. In order to obtain a FIB carbon deposition with a similar chemical composition, I would have to look for methods of raising oxygen concentration that were external to the FIB.

3.2 Effect of Heat upon FIB Carbon Depositions

I also found that the concentration of oxygen could be increased by exposure to heat. Using the Thermolyne® 21100 Tube Furnace, I was able to expose the FIB carbon depositions to a variable temperature between 100 ºC to 1,200 ºC. I first studied the effects of 500 ºC heat as an arbitrary temperature. Not only did the oxygen increase, but concentration of gallium in the sample *decreased.* The concentrations of oxygen and gallium in a single sample as a function of its exposure to 500 ºC heat is plotted in Figure 7. The decrease in the concentration of gallium is likely due to the formation of gallium oxide balls in the corners of the carbon deposition, which can be seen in Figures 8a and 8b. The gallium has a melting point just above room temperature. When exposed to such high temperatures, the gallium seems to have secreted, oxidized, and then collected in the corners.

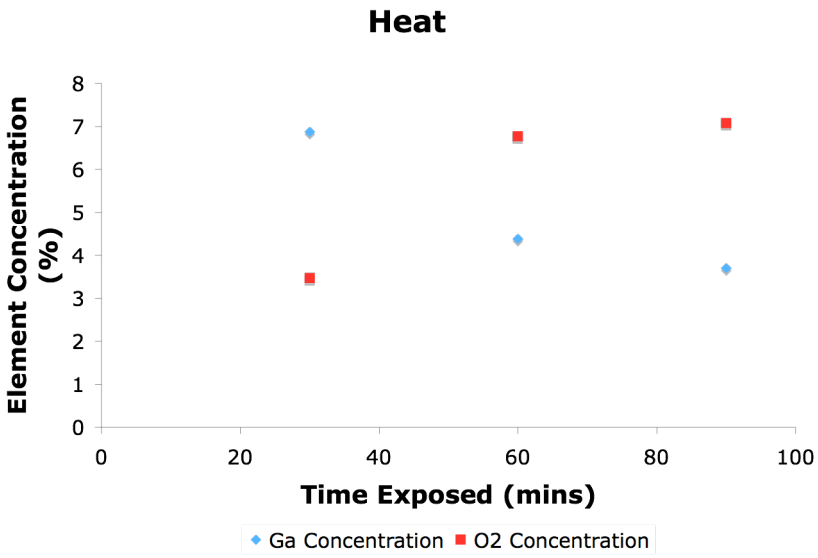

Figure 7

Concentration of oxygen (pink squares) and Gallium (black triangles) in a single sample exposed to 500 ºC heat in the tube furnace. Notice that the oxygen concentration increased in the sample while the gallium concentration decreased.

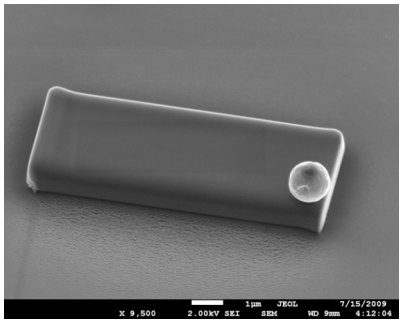

Figure 8a

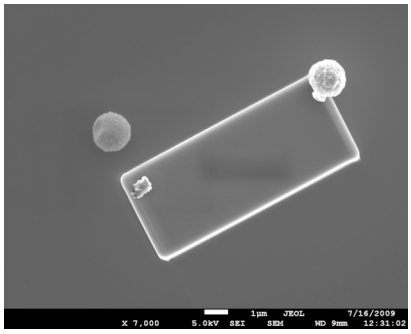

Figure 8b

Figure 8a shows a ball of cooled gallium at a corner of a FIB carbon deposition that grew after 30 minutes of exposure to 500 degrees Celsius. Figure 8b shows the same deposition after 30 additional minutes of exposure. The first ball fell off while a second one grew on another corner.

A sample exposed to 700 ºC for 30 minutes exploded, which can be seen in Figure 9. Two samples exposed to 300 ºC for 60 minutes had minimal effect on the concentration of oxygen in the sample. Due to the results of these tests, further exposure of FIB carbon depositions to heat remained at 500 ºC.

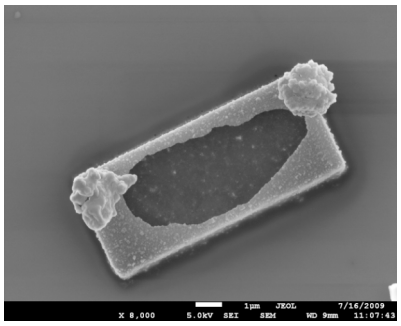

Figure 10

Figure 9 is an image of the carbon deposition that exploded after 30 minutes of exposure at 700 Celsius. The dark blob in the middle of the carbon deposition is actually the crater formed from the explosion. Note also how two gallium bubbles have formed on the corners of the deposition.

3.3 Effect of Oxygen Plasma upon FIB Carbon Depositions

Plasma is a state of matter that describes a gas whose particles are ionized. I found that exposing samples to the oxygen plasma increased their concentration of oxygen. I used the PS210 Microwave Plasma System to bring the samples in contact with oxygen plasma. Figure 6 is a plot of the oxygen concentrations in eleven separate samples versus the time each sample was exposed to plasma. It indicates that exposure to oxygen plasma achieves a maximum oxygen concentration after about fifty-five minutes and then plateaus after further exposure. Further study showed that exposure to the plasma system must occur in fifteen or twenty minute stages: Two samples that were exposed for an hour without pause showed an oxygen concentration of only 3.85% and 3.73%.

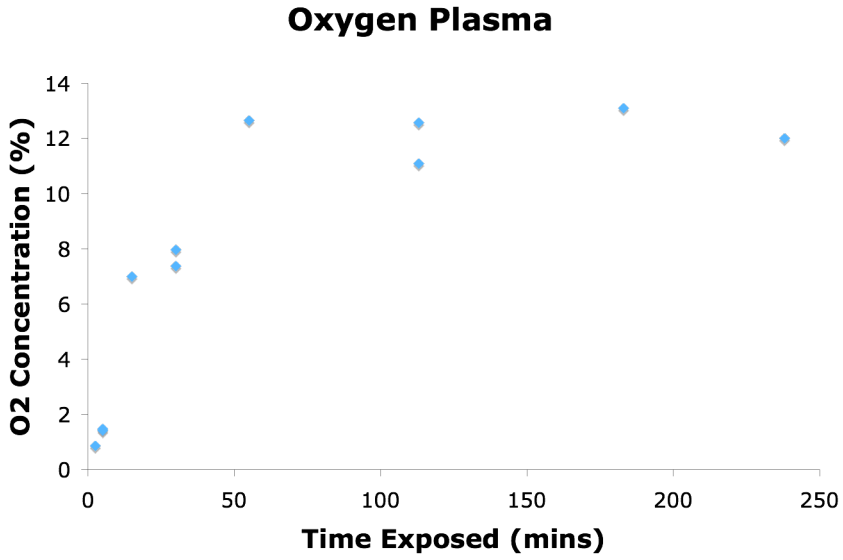

Figure 6

Concentration of oxygen found in FIB carbon depositions plotted as a function of total time exposed to oxygen plasma. Note that the same concentration of oxygen is maintained after 55 minutes of exposure.

Two samples exposed for five minutes had very similar concentrations: 1.42 and 1.47

It should be noted that in six of the eleven samples plotted in Figure 7, a concentration of 3.6 % ± 0.2 % fluorine was found. The source of fluorine is unknown and did not occur in other samples exposed to the oxygen plasma. It does not appear that fluorine concentration affected the concentration of oxygen in the sample.

3.4 Effects of Heat and Oxygen Plasma on FIB Carbon Depositions

Combining exposure to plasma and to heat consistently produced the highest concentrations of oxygen in FIB carbon depositions. After being exposed to the plasma microwave system for 113 minutes followed by the furnace for 30 minutes at 500 ºC, the sample on the left of Figure 10 was found to have 20.29 % Oxygen.

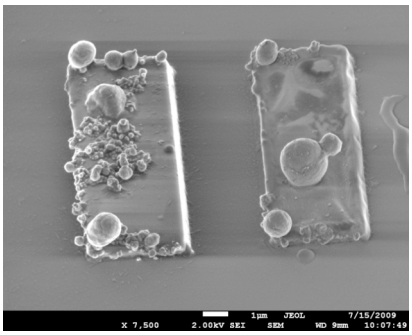

Figure 10

Carbon deposition on the left was found to have an oxygen concentration of 20.29% after being exposed to both oxygen plasma and heat. The sample on the right is not important.

A different sample that had been exposed to sixty minutes of plasma and then sixty minutes of 500 ºC heat had a concentration of 20% oxygen. Yet another sample had a concentration of only 14.75 % oxygen when exposed to forty-five minutes of plasma followed by sixty minutes of 500 ºC heat. To conclude, combining the methods of plasma exposure and heat exposure consistently increased the concentration of oxygen in a sample that was higher than either method could achieve without the other. No sample, however, achieved the 37.5 % oxygen concentration observed in Dhakal's superconducting sample.

3.5 Determining Superconductivity

In order to determine the presence of superconductivity in a sample, a four-point probe was used to measure its resistance when it was lowered into a dewar of liquid helium. Liquid helium boils at 4.2 K, which is lower than the observed 7 K temperature transition to superconductivity in the superconducting FIB carbon deposition. A four-point probe measurement consists of measuring the voltage across a resistor while a constant current is supplied. By dividing the measured voltage drop by the known current supplied, I can precisely measure the resistance without contribution from the internal resistance of the instrumentation is obtained. For this measurement, a larger 40

micrometer x 4 micrometer carbon deposition with a dose of 3 nc/μm^2 was deposited across the probe's four wires, as depicted in Figure 11.

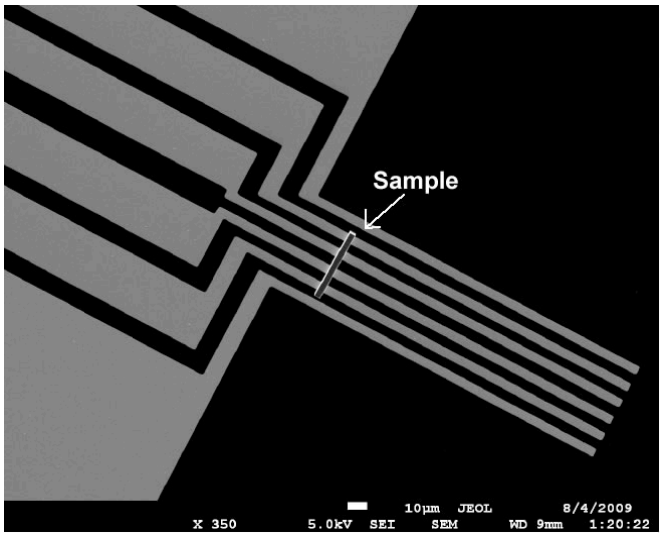

Figure 11

FIB carbon deposition placed across four of six golden wires that extend off towards the upper left corner.

After fifty minutes of exposure to oxygen plasma, consisting of two fifteen minute stages followed by one twenty minute stage, the sample was measured to have a concentration of oxygen of 23.35%. An additional sixty minutes of exposure raised the concentration of oxygen to 25%. The fact that 23.35% oxygen could be achieved through only exposure to plasma was surprising, but it is likely because the larger sample had a greater surface area across which the plasma could dope the deposition. However, despite this increased concentration of oxygen, the helium dip showed that the 25% oxygen sample was not a superconductor.

3.6 Concluding Remarks on FIB Depositions

The goal of this project was two-fold: first, to raise the oxygen concentration in FIB carbon depositions and secondly, to see if such oxygen doped samples would be superconducting. The highest concentration of oxygen in a sample was 25%. Two methods were employed to achieve this: exposure to oxygen plasma and heating within a tube furnace. The oxygen concentration in a sample after heating a sample within a tube furnace would typically peak to about 8% after about 60 minutes. The effect of plasma on FIB carbon depositions was investigated to show that maximum oxygen concentration—about 12%—was achieved after about fifty-five minutes of exposure. The 25% oxygen concentration sample was achieved by a combination of exposure to oxygen plasma and heating in the tube furnace.

A number of future studies can stem from the research presented here. Despite the lack of superconductivity in a 25% oxygen FIB carbon deposition, additional methods of oxygen doping should be researched as it may aid efforts of creating a sample with 40% oxygen. Repeatedly exposing a sample to plasma followed by heat may drive energetically deposited plasma oxygen deeper into the material. Perhaps a sample with a

larger surface area than what was described in Section 3.5 would yield an even larger concentration of oxygen. Also, efforts in creating a sample with a higher gallium concentration may result in a superconducting FIB carbon deposition.

4.0 Exploring the Superconducting State of $(TMTSF)_2ClO_4$

In contrast to oxygen-rich carbon, which was first suspected to be superconducting in 2008, $(TMTSF)_2ClO_4$ has long been known to be superconducting. As a result, its chemical and crystallographic structure have long since been characterized. This understanding leads to the surprising prediction that its Cooper pairs would have net spin $s = 1$ rather than the typical $s = 0$ found in other superconductors. While this proposal has received much experimental theoretical scrutiny, experiments have been inconclusive as to the true nature of the superconductivity in $(TMTSF)_2ClO_4$. For the summer of 2008, I worked with Dr. Naughton's group at Boston College to characterize the organic crystal's superconductivity. More specifically, I prepared samples of $(TMTSF)_2ClO_4$ for tunneling current measurements that could determine the net spin of the Cooper pairs in the material.

In the following sections, I describe Josephson junctions qualitatively and quantitatively in Section 4.1, I describe the various forms of Cooper pairing in Section 4.2, and I describe how Josephson junctions can be used to determine the form of Cooper pairing present in a superconductor in Section 4.4. Section 4.3 serves as an introduction to $(TMTSF)_2ClO_4$. In Section 4.5, I present the details of my successful cleaving of the $(TMTSF)_2ClO_4$ organic superconductor and my attempts to form a Josephson junction across its a-axis. I then offer some concluding remarks in Section 4.6.

4.1 Josephson Junction

The wavefunction of a superconductor, ψ, is historically referred to as the order parameter. The following derivations first describe the quantum mechanics of a local current density followed by both a qualitative and a quantitative description of the direct current Josephson effect.[2]

An electron experiences a momentum, ***p***,

$$\vec{p} = m\vec{v} \qquad \textit{Equation 7}$$

where m is the mass of the electron and ***v*** is its velocity. In quantum mechanics, operators are used to describe physical values. The operator for momentum is $\hat{p} = -i\hbar\vec{\nabla}$, where $\hbar$ is Planck's constant divided by 2π. To find the operator for kinetic energy, we start with its classical definition and substitute the quantum mechanical operators to get

$$K = \frac{1}{2}mv^2 = \frac{1}{2m}\left(\vec{p}\right)^2 \rightarrow \frac{1}{2m}\left(-i\hbar\vec{\nabla}\right)^2 = \hat{K}.$$

Expanding the squared term gives

$$\hat{K} = -\frac{\hbar^2}{2m}\vec{\nabla}^2. \qquad \textit{Equation 8}$$

The contribution of the electron to the electric current is given by the expectation value of

[2] Please note that these derivations are borrowed very heavily from Hook and Hall, 1991 pp. 296-298, pp. 304-306 and pp. 430-431

$$-e\vec{v} = -\frac{e}{m}(\vec{p}). \qquad \textit{Equation 9}$$

where e is the charge of the electron. That is, by the integral

$$I = -\int\left(\frac{e}{2m}\left[\psi^*(-i\hbar\vec{\nabla})\psi + \psi(i\hbar\vec{\nabla})\psi^*\right]\right)dV \qquad \textit{Equation 10}$$

The integrand can be interpreted as the local current density $\boldsymbol{j}$ associated with the wavefunction ψ. Hence,

$$\vec{j} = \frac{i\hbar e}{2m}(\psi^*\vec{\nabla}\psi - \psi\vec{\nabla}\psi^*). \qquad \textit{Equation 11}$$

This current density satisfies conservation of probability when ψ satisfies Schrödinger's time-dependent equation

$$\hat{K}\psi = i\hbar\frac{\partial\psi}{\partial t}. \qquad \textit{Equation 12}$$

For a Cooper pair, two electrons are considered a single particle, so $e \rightarrow 2e$ and $m \rightarrow 2m$ giving a cooper pair current density of

$$\vec{j} = \frac{i\hbar e}{2m}(\psi^*\vec{\nabla}\psi - \psi\vec{\nabla}\psi^*). \qquad \textit{Equation 13}$$

The most general form of ψ can be described as a simple wave,

$$\psi(\vec{r}) = |\psi(\vec{r})|e^{i\theta(\vec{r})}. \qquad \textit{Equation 14}$$

Where the magnitude of the order parameter may be normalized to be the number of Cooper pairs, which can be represented as

$$|\psi(\vec{r})|^2 = \frac{n_s}{2}. \qquad \textit{Equation 15}$$

Here n_s is the number of superconducting electrons. Half of n_s gives the number of Cooper pairs.

Now consider two superconductors separated by only a few angstroms. Such a configuration is referred to as a Josephson junction. Cooper pairs, like electrons, may tunnel across this boundary and create a current. Unlike electrons, however, a current will flow across the Josephson junction *without any applied electric potential*. This phenomenon is referred to as the DC Josephson effect.

The superconductors in Figure 14 form such a Josephson junction. Separated by a distance of d, the superconductors on the left and right have order parameter $\psi_1 = |\psi_1|e^{i\theta_1}$ and $\psi_2 = |\psi_2|e^{i\theta_2}$, respectively. Notice that the phases for the two superconductors will be treated as constants that are not necessarily the same. Equation 16 describes the phase, θ, as a function of position so as not to limit its use. When describing conventional superconductors and the ones in this paper, θ can be considered constant throughout a homogenous, connected material. If a substantial portion of the surface of the two superconductors meet, the phases of the two superconductors will become the same and no DC Josephson effect would be observed upon being pulled apart again. The reasons for this will be made clear in a moment.

Figure 14

Josephson junction consisting of two superconductors with a simple barrier in between them. The barrier has width d and extends from $x = -d/2$ to $x = +d/2$.

For the purpose of this presentation, we assume that the order parameters of the two superconductors significantly overlap only in the barrier region. That is, the order parameter of the superconductor on the right will be too small to be considered at the position of the superconductor on the left and vice versa, as seen in Figure 15. In the barrier, the order parameter that describes the probability of detecting the presence of a Cooper pair takes into account tunneling from both superconductors. Hence the order parameter will be a combination of the two superconductors' order parameters. As is typical with tunneling phenomenon, the probability of detecting a Cooper pair in a potential barrier decays exponentially as the distance from its respective superconductor increases.

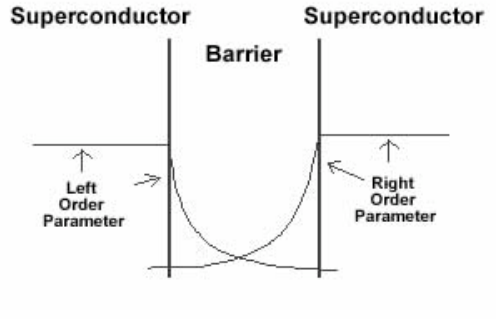

Figure 15

Sketch of the order parameter's decay in the potential barrier of the Josephson junction.

Thus the order parameter within the barrier is

$$\psi = |\psi_1| e^{i\theta_1} e^{-K(x+d/2)} + |\psi_2| e^{i\theta_2} e^{+K(x-d/2)} \qquad \textit{Equation 16}$$

where ψ_1 is the order parameter on the left, ψ_2 is the order parameter on the right, and K^{-1} is the characteristic length of decay of the order parameter within the barrier. Since both identical superconductors are cooled to the same temperature below their respective critical temperatures, the density of cooper pairs should be the same in both materials, so Equation 17 gives $|\psi_1|^2 = |\psi_2|^2 = n_s/2$. This gives

$$\psi = (n_s/2)^{1/2} \left(e^{i\theta_1 - K(x+d/2)} + e^{i\theta_2 + K(x-d/2)} \right) \qquad \textit{Equation 17}$$

Now, substituting Equation 19 into Equation 15, we have an expression for the DC Josephson effect:

$$j = \frac{ie\hbar n_s}{2m} K e^{-Kd} \left(-e^{i(\theta_1 - \theta_2)} + e^{i(\theta_2 - \theta_1)} \right) \qquad \textit{Equation 18}$$

This can be greatly simplified to describe what's important:

$$j = j_0 \sin(\delta) \qquad \textit{Equation 19}$$

Where $j_0 = e\hbar n_s K \exp(-Kd)/m$ and $\delta = \theta_1 - \theta_2$ is the phase difference between the two sides of the junction. Notice that if the two sides have equal phase, no Josephson current would be observed. For the purpose of this paper, the most important dependance is j_0's dependance on n_s, the density of Cooper pairs. In an isotropic material, one would expect Cooper pairs to be equally likely to form between electrons with equal and opposite momentum along *any* direction, should the temperature be cool enough. In contrast, in an anisotropic material, Cooper pairs may more easily form in one direction than in another, and that preference may itself be temperature dependant. With different possible $n_{s,}$, and therefore ψ, symmetries come different possible angular momenta and spins.

4.2 Triplet Superconductivity

The symmetry, angular momentum, and net spin of Cooper pairs distinguish the different possible superconducting states, a difference that yields observable effects on the Josephson currents. Electrons in an atom have angular momentum analogous to (but not the same as) the conserved property related to orbiting bodies described in classical mechanics. Three numbers are used to describe the state of an electron: the principal quantum number n, the azimuthal quantum number l, and the magnetic quantum number j[3]. The energy associated with the electron is related to its particular n, while l and j are related to its angular momentum. The number n is any positive nonzero integer (n = 1, 2, 3, …), l is any integer up to n (l = 0, 1, 2, …, n – 1), and j ranges from $-l$ to l in integer steps (j = -l, -l + 1, ..., l – 1, l). The magnitude of a single electron is measured to be

$$L^2 = \hbar^2 l(l+1) \qquad \textit{Equation 20}$$

A component of the angular momentum of single electron is

$$L = \hbar j \qquad \textit{Equation 21}$$

Electrons are particles that also have a spin[4], s, of ½. Similar to angular momentum, the magnitude of the spin of a single electron is measured to be

$$S^2 = \hbar^2 s(s+1) \qquad \textit{Equation 22}$$

The component of the spin of the electron depends on the quantum number m that ranges from -s to +s in integer steps and will be measured to be

$$S = \hbar m \qquad \textit{Equation 23}$$

The spin state of a given electron can be represented in several notations. The general formulation is that a particle with spin s and quantum number m is in state $| s\ m >$. But since m is only one of two values, it can be either spin "up" and spin "down" represented by ↑ and ↓, respectively. To be rigorous, $| ½\ -½ > = \downarrow$ and $| ½\ +½ > = \uparrow$.

When considering two electrons in a system such as phonon coupling, the four possible configurations are

$$\uparrow\uparrow, \uparrow\downarrow, \downarrow\uparrow, \downarrow\downarrow$$

In this case, the quantum number of the system, m_{tot} is defined to be the sum of the quantum numbers of each electron. When considering the above spin configurations, we can calculate m_{tot} as

[3] Typically, the magnetic quantum number is referred to as m. I am saving this letter, however, for the quantum number associated with spin.

[4] Note that it is dangerous to use the term *spin*—electrons should never be considered to spheres spinning in space.

$$\uparrow\uparrow: m_{tot} = 1$$
$$\uparrow\downarrow: m_{tot} = 0$$
$$\downarrow\uparrow: m_{tot} = 0$$
$$\downarrow\downarrow: m_{tot} = -1$$

If we were to consider the pair of electrons to be akin to a single particle with a new spin of s_{sys} it would be desirable for the m_{sys} to be arranged from $-s_{sys}$ to $+s_{sys}$ in integer steps just like that in a single electron. The above spin configurations do not, unfortunately, go from $-s_{sys}$ to $+s_{sys}$ in integer steps because there are two m_{tot} states. It can be shown that $\uparrow\uparrow$ and $\downarrow\downarrow$ have $s_{sys} = 1$, so we can apply the raising/lowering operator

$$S_{\pm}|sm\rangle = \hbar\sqrt{s(s+1) - m(m\pm 1)}\,|s(m\pm 1)\rangle \qquad \textit{Equation 24}$$

to find a term that we assign as having a total quantum number, m_{tot} of zero. To clarify: applying the lowering operator to the state with $m_{tot} = 1$ and the raising operator to the state with $m_{tot} = -1$ should both give a state with $m_{tot} = 0$. If the lowering operator of the system of particles is equal to the sum of the lowering operator of each individual particle[5], the lowering operator of the system on $\uparrow\uparrow$ gives

$$S_{-}(\uparrow\uparrow) = \left(S_{-}^{\,1}\uparrow\right)\uparrow + \uparrow\left(S_{-}^{\,2}\uparrow\right)$$
$$S_{-}(\uparrow\uparrow) = \hbar(\downarrow\uparrow + \uparrow\downarrow)$$

Applying the raising operator to $\downarrow\downarrow$ gives the exact same thing. Hence the three states with $s_{sys} = 1$ are

$$|11\rangle = \uparrow\uparrow$$
$$|10\rangle = \frac{1}{\sqrt{2}}(\uparrow\downarrow + \downarrow\uparrow) \qquad \textit{Equation 25}$$
$$|1-1\rangle = \downarrow\downarrow$$

Hence, the "triplet state[6]" refers to a pair of electrons with $s_{sys} = 1$. By similar reasoning, the $s_{sys} = 0$ state, which is referred to as the "singlet state," is

$$|00\rangle = \frac{1}{\sqrt{2}}(\uparrow\downarrow - \downarrow\uparrow) \qquad \textit{Equation 26}$$

Notice that applying either the raising or the lowering operator to the singlet state results in zero, which is what we would expect.

The type of superconductivity of a Cooper pair is determined by its angular momentum. If the Cooper pair's angular momentum is zero, the superconductivity is referred to as "s-wave." If it is measured to be $\hbar$ or $2\hbar$, the superconductivity is referred to as "p-wave" or "d-wave," respectively (Ishiguro and Yamaji, 1990, p. 176-177). S-wave and d-wave superconductors have Cooper pairs in the singlet configuration, while p-wave superconductors have their Cooper pairs in the triplet configuration. BCS Theory, which explains conventional Type I superconductors quite well, describes Cooper pairs to take on the singlet "s-wave" configuration. Triplet superconductivity is a novel form of Cooper pairing that has been suggested to occur by only a handful of experiments.

[5] This argument has been borrowed heavily from (Griffiths, 2005, pp. 171-174 and 184-189)

[6] Note that triplet state actually refers to three states: |1 1 >, |1 0 >, and |1 -1 >.

4.3 The Organic Crystal $(TMTSF)_2ClO_4$

$(TMTSF)_2X$ (where X = ReO_4, ClO_4, BF_4, PF_6, AsF_6, etc.) is a member of the Bechgaard salts family, which means that it is a fullerene consisting of a tetrathiolfulvalene core as illustrated in Figure 12. "TMTSF" in $(TMTSF)_2X$ is an abbreviation for **t**etra**m**ethyl**t**etra**s**elena**f**ulvalene.

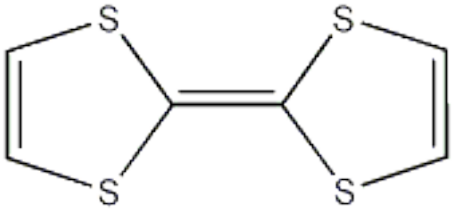

Figure 12

The tetrathiolfulvalene core of the Bechgaard salts. Notice that the molecule is planar and highly anisotropic. In TMTSF, the sulfur atoms are replaced with selenium ones.

The organic crystal is triclinic, meaning that the vectors that describe the mapping of the crystal structure are unequal and not orthogonal. Figure 13a details the structure of TMTSF, while Figure 13b gives the three dimensional structure of $(TMTSF)_2ClO_4$, the organic superconductor that is of particular interest in this paper. Referring to Figure 13a, the axis a, b, c, are *roughly* out of the page, from top to bottom, and from left to right, respectively. The conductivity along the a-axis is ten times greater than that of the b-axis, which, in turn, is ten times greater than of the c-axis. Due to this fact, $(TMTSF)_2ClO_4$ is considered a "quasi-one dimensional" material since the electrons feel roughly only one-dimension of conductivity. Bechgaard salts also exhibit atomic-spin orientation preferences with antiferromagnetic and spin density phases (W. Zhang and C. Sa de Melo, 2007). This spin orientation preference and quasi-one dimensionality is very suggestive that Cooper pairs should have a state that is fairly one dimensional and has net spin, i.e. p-wave superconductivity.

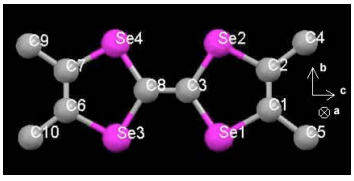

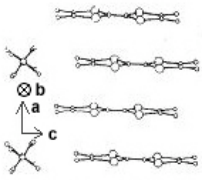

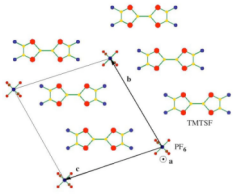

Figure 13a *Figure 13b* *Figure 13c*

Figure 13a shows a two dimensional perspective of the TMTSF cation. The crystalline axis that the molecules form along are a, b, and c, which point into the page, *roughly* top to bottom, and *roughly* left to right, respectively. Figure 13b shows a three dimensional perspective of $(TMTSF)_2ClO_4$. The overlapping orbitals cause the highest conductivity along the a axis of the crystal. (Rindorf et al., 1982) Figure 13c gives a more accurate representation of the angles between the crystal axes. (W. Zhang and C. Sa de Melo, 2007)

4.4 Characterizing Superconductivity Through Josephson Currents

A plot of the Josephson DC current as a function of temperature can distinguish between s-wave, p-wave, and d-wave superconductivity in a given material. For any Josephson junction, Equation 22 can be rewritten as a ratio between the energy gap and a

theoretical resistance referred to as the normal resistance of the junction, R_N (Ambegaokar and Baratoff, 1963):

$$j = \frac{\pi}{2}\frac{\Delta(T)}{eR_N} \qquad \textit{Equation 27}$$

Equation 27 can be thought of as a "rephrasing" of j from equation 19 in terms of the energy gap, Equation 6, rather than n_s. The energy gap as a function of temperature for an s-wave superconductor is well known (Equation 6) and it can be sketched to have the same curve as Figure 5, as can be seen in Figure 16. The normalization, in this case, would be different: $\pi\Delta_0/2eR_N$, where Δ_0 is the energy gap at absolute zero instead of just Δ_0. The important features of Figure 16 are that the concavity of the curve is downward and that it approaches singularity in the limit of zero temperature.

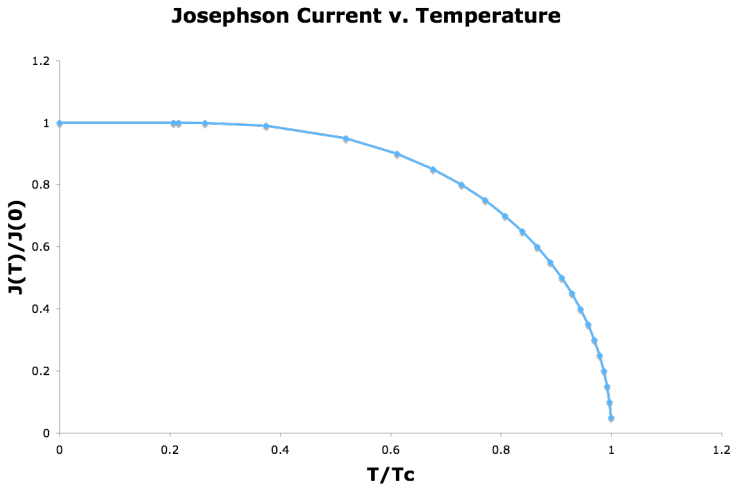

Figure 16

Josephson current for s-wave superconductor as a function of temperature. Since the Josephson current of an s-wave superconductor varies directly with the energy gap, Figure 16 has the same curvature as Figure 5. Note that, given the normalization of $\pi\Delta_0/2eR_N$, the measured Josephson current goes to singularity as the temperature goes to zero. Also note that concavity of the curve is downward.

Asano et al. published a paper describing the Josephson currents for $(TMTSF)_2ClO_4$ considering it as p-wave or as a d-wave superconductor. When using the Hubbard model to calculate this current profile, a parameter called a "hopping integral" is used to describe the probability of an electron tunneling, or "hopping" from one positive ion to the an adjacent one. The hopping integral has units of energy because of the kinetic energy of the moving electron that it represents. In $(TMTSF)_2ClO_4$, the a-axis is about ten times more conductive than the b-axis, so the hopping integral along the a-axis, t_a, compared to the one along the b-axis, t_b, is $t_a = 10t_b$. The c-axis is neglected for its poor conductivity and is not represented with a hopping integral. Asano et al. introduce a third hopping integral, t', between the next nearest neighbors is to allow them to explore the possibility of diagonal conduction. The arrangement of these hopping integrals can be represented as in Figure 17. Notice that while t_a and t_b are orthogonal, t' is a diagonal hopping integral to account for the triclinic nature of $(TMTSF)_2ClO_4$. As can be seen from

Figure 18, the Josephson junction can be arranged so that the *t'* hopping integral direcction is either parallel on both sides or forms a mirror image across the junction.

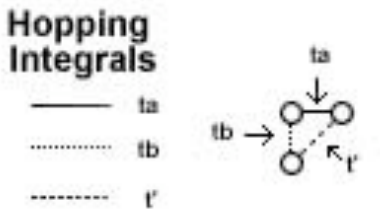

Figure 17

The hopping integrals between superconducting atoms (circles) in $(TMTSF)_2ClO_4$ can be represented by lines between each atom. Since the a-axis is ten times more conductive than the b-axis, $t_a = 10t_b$. The hopping integral along the c-axis does not need to be considered because the c-axis is one tenth less conductive than the b-axis and so is negligible.

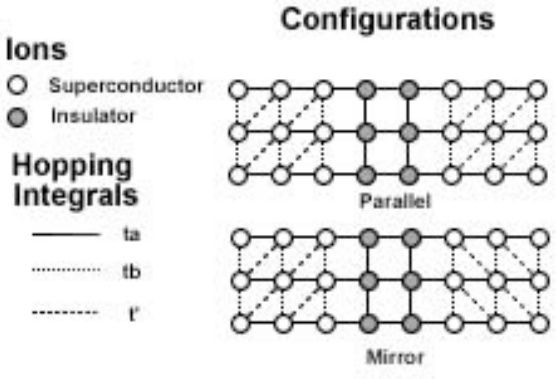

Figure 18

The top of the image represents a Josephson junction with parallel *t'* hopping integrals. The bottom of the image represents a Josephson junction with mirrored *t'* hopping integrals. (Adapted from Asano et al., 2004)

The theoretical plot of p-wave superconducting Josephson current as a function of temperature is depicted in Figure 19. The figure shows that *t'* does not have a significant impact on the shape or magnitude of the current versus temperature profile of the p-wave superconductivity. According to Asano et al., the resulting Josephson current v. temperature profile is the same regardless of whether the Josephson junction is a mirror-type or parallel-type junction. The distinguishing characteristic of the p-wave Josephson current profile is that is concave upwards and is much larger than that of an s-wave superconductor.

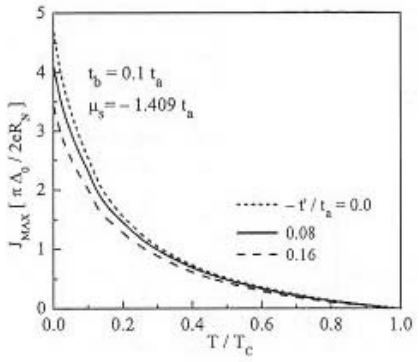

Figure 19

Josephson current of a p-wave quasi-one dimensional superconductor as a function of temperature. t_a and t_b refer to the hopping integrals along the a and b axis, respectively, while t' refers to the hopping integral between every other ion. Notice that the curvature of the current profile is concave up and is five times larger than an s-wave Josephson current at absolute zero. (Asano et al., 2004)

The theoretical plot of d-wave superconducting Josephson current as a function of temperature is depicted in Figure 20a and 20b. Here, the configuration of the Josephson junction is significant if the material is a d-wave superconductor. The parallel configuration is depicted in Figure 20a while the mirror configuration is depicted in Figure 20b. The distinguishing features about the d-wave Josephson current profile is that it is concave upwards and is much smaller than that of an s-wave superconductor. The *t'* hopping integral is of significance in the d-wave Josephson junction, resulting in significant changes in the quantity and curvature of the Josephson current profile's curve. Notice that the type of superconductivity in a material is easily discerned by examining the concavity of the Josephson current v. temperature profile.

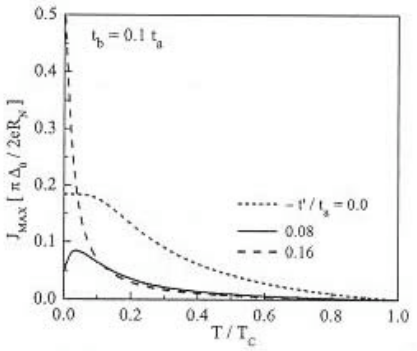

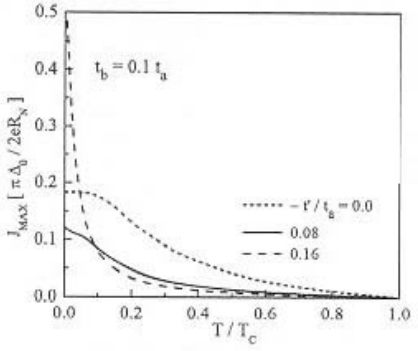

Figure 20a *Figure 20b*

Josephson current profiles in a d-wave superconductor. Figure 20a is the Josephson current of a d-wave superconductor in the parallel configuration as a function of temperature, while Figure 20b is that of a mirror configuration. Notice that the curvature of the current profile is

concave up and has a magnitude that is less than half an s-wave Josephson current at absolute zero. (Asano et al., 2004)

4.5 Preparing the Josephson Junction

We were interested in creating a Josephson junction along the a-axis of $(TMTSF)_2ClO_4$. Unfortunately, the crystals grow primarily along this very axis and so they must be cleaved to obtain a clean bc-plane. The problem was that $(TMTSF)_2ClO_4$ is extremely difficult to handle. Very brittle, the organic crystal can snap and/or crack due to very small macroscopic forces. For example, to transfer the crystals from a container to the stage of a microscope, we used the static electricity of an insulator that had been rubbed through fur to pick up the sample.

This paper reports the first successful cleavage of $(TMTSF)_2ClO_4$ in the Naughton lab at Boston College, as depicted in Figure 21a and 21b. Cleaving the crystal was achieved by attaching a wooden splinter "post" with non-destructive silver paste to the side of the organic crystal as depicted in Figure 22. Since the crystal had already been mounted onto a surface, again with silver paste, minor forces that were repeatedly applied to the post would cause the crystal to cleave due to torsional strain.

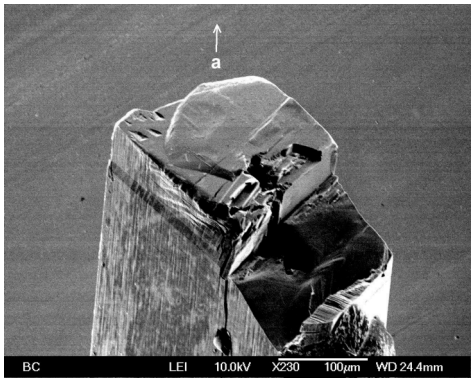

Figure 21a

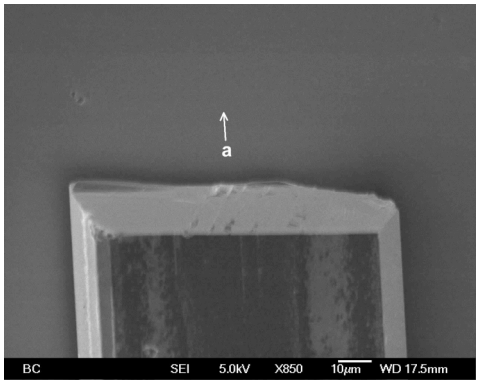

Figure 21b

Cleaved surfaces of two $(TMTSF)_2ClO_4$ organic crystals. Figure 21a gives a clear view of the bc plane from an angle. Figure 21b is a profile of the bc plane with the a-axis pointing up.

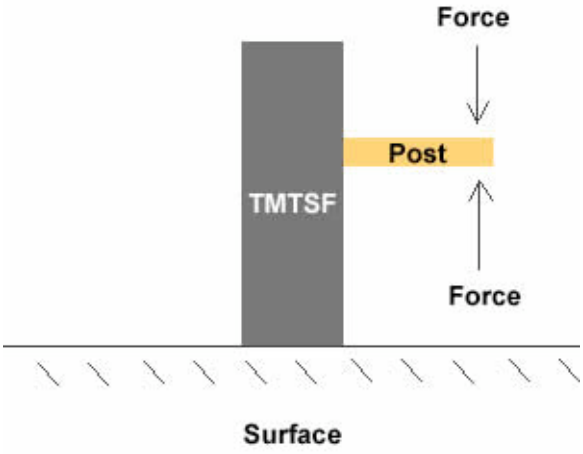

Figure 22

$(TMTSF)_2ClO_4$ was cleaved by attaching a wooden splinter "post" to the side of a crystal that had been mounted to a surface. Force was then repeatedly applied to the end of the post. All junctions were made using the non-destructive adhesive silver paste. To give a sense of scale, the lengths of both crystal and the post were on the order of centimeters.

Upon creating the cleaved surface, we made three attempts to create a Josephson junction. The first two involved sputtering gold upon the cleaved surface to create the conducting barrier as depicted in Figure 23a. The third involved growing $(TMTSF)_2PF_6$, crystals upon the cleaved surface as the normal conducting barrier, as depicted in Figure 23b. $(TMTSF)_2PF_6$ is another Bechgaard with the same TMTSF cation core but with a phosphorus hexafluoride anion instead of perchlorate. At ambient pressure, it is a normal conductor. On all three samples, a final layer of $(TMTSF)_2ClO_4$ was added. Hence all three were supposed to achieve Superconductor-Normal-Superconductor Junctions.

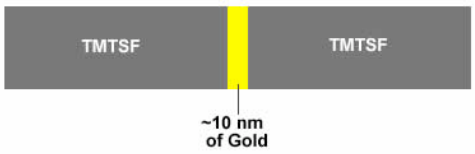

Figure 23a

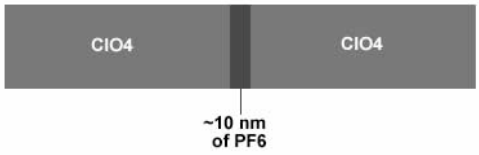

Figure 23b

Intended Josephson junctions. In Figure 23a, two $(TMTSF)_2ClO_4$ superconductors are separated by about ten nanometers of gold. In Figure 23b, two $(TMTSF)_2ClO_4$ are separated by a ten nanometer span of $(TMTSF)_2PF_6$, which is a normal conductor at ambient pressure.

Unfortunately, as can be seen from Figures 24a, 24b, and 24c, the Josephson Junctions were unsuccessful. When attempting to create the Josephson junctions off the sputtered gold, the $(TMTSF)_2ClO_4$ crystals did not grow on *only* the gold. Instead, it had

short-circuited the gold Josephson junction and simply created a single continuous crystal off of the original $(TMTSF)_2ClO_4$. The Josephson junction intended with the $(TMTSF)_2PF_6$ was also unsuccessful because the $(TMTSF)_2PF_6$ grew too long. The Josephson junction needs to be on the order of nanometers but, as can be seen in Figure 24c, the $(TMTSF)_2PF_6$ is on the order of centimeters.

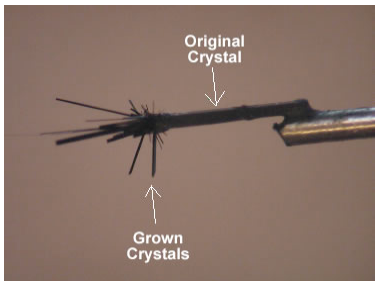

Figure 24a

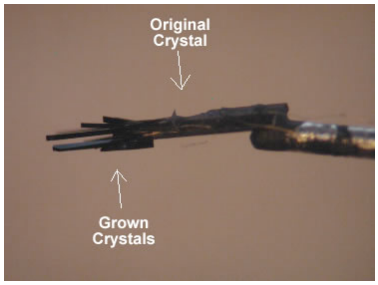

Figure 24b

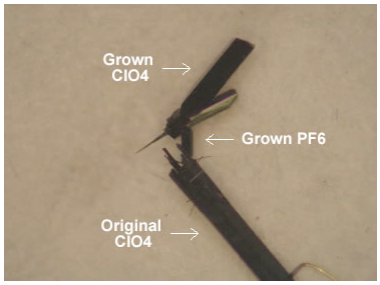

Figure 24c

Figures 24a and 24b are attempts to create Josephson junctions as shown in Figure 23a held by a probe on the right. The multiple crystals that have grown on the left end of the crystal have probably short circuited the gold Josephson junction. Figure 24c is an attempt to create a Josephson junction as shown in Figure 23b. Notice that the adjoining $(TMTSF)_2PF_6$ junction is macroscopically visible and therefore not on the necessary order of nanometers to form a Josephson junction. To give a sense of scale, the length of crystals are on the order of centimeters.

4.5 Concluding Remarks On Josephson Junctions

I was able to cleave the organic crystal $(TMTSF)_2ClO_4$ by adhering a post to the side of the crystal and applying torsional force. I then attempted to make Josephson junctions using three cleaved surfaces. The barrier along two of the crystals was supposed to be sputtered gold while the barrier along the third crystal was supposed to be $(TMTSF_2)PF_6$, which is a normal metal at ambient pressures. None of the Josephson junctions were successfully formed because no manner of control could be exhibited upon crystal growth. For the junction made of sputtered gold, the crystals grew around the gold barrier to circumvent the formation of a Josephson junction. No control could be exerted for *where* the crystals grew. With the junction made of $(TMTSF)_2PF_6$, the $(TMTSF)_2PF_6$ crystal grew far too long for the Josephson junction to form. No control could be exerted for *how long* the crystal grew. In order to successfully form a Josephson junction using $(TMTSF)_2ClO_4$, further research must be made into controlling crystal growth.

5.0 Conclusion

In the first project discussed, I worked on reproducing a newly reported and unexpected oxygen-rich carbon superconductor fabricated by FIB deposition. In particular I explored ways to increase the oxygen concentration. I was able to raise the oxygen concentration in samples by exposing them to heat and oxygen plasma. By exposing a sample to heat, I was able to increase the oxygen concentration to about 7 % whereas I was able to increase the oxygen concentration to 12 % using plasma. Additionally, the concentration of gallium was found to decrease through exposure to

heat. Using a combination exposure of heat and plasma, I raised the oxygen concentration in a sample to 25 %. Unfortunately, the 37.5 % concentration that was reported for the superconducting sample was not achieved; the 25% concentration sample did not demonstrate superconductivity. Additional research should investigate methods of further increasing the concentration of oxygen or increasing the concentration of gallium in FIB carbon depositions. Additional research should be conducted to see if exposure to heat would decrease the concentration of gallium in FIB tungsten deposits to see if conductivity might be improved.

In the second project discussed, I worked on creating a Josephson junction with the organic superconductor $(TMTSF)_2ClO_4$ to see if the Josephson current as a function of temperature would have a profile indicating novel forms of superconductivity. I was able to cleave the organic superconductor, $(TMTSF)_2ClO_4$ along the b- and c- axes so that the a-axis was exposed for the formation of a Josephson junction. I made three attempts at creating such a Josephson junction: two involved sputtering gold onto the cleaved surface and one involved growing $(TMTSF)_2PF_6$ off of it. None of my attempts to form a Josephson junction were successful because I could not control where or how long the crystals would grow. Progress in the experiment is contingent upon developing methods to control the manner in which $(TMTSF)_2X$ crystals grow.

Together these two projects provide two snapshots of the often multi-decade progression from the first observation of superconductivity in a material to the full understanding of the superconductivity state and the underlying mechanism.

References

1. A. Abrikosov, *Fundamentals of the Theory of Metals*. (Physical Sciences and Engineering Division, Amsterdam, 1988)
2. V. Ambegaokar and A. Baratoff, "Tunneling Between Superconductors" Physical Review Letters **10** 11 (1963)
3. Y. Asano, Y. Tanaka, Y. Tanuma, K. Kurkoki, and H. Tsuchiura, "Josephson Effect in Quasi One-dimensional Unconventional Superconductors."
4. S. Belin and K. Behnia, "Thermal Conductivity of Superconducting $(TMTSF)_2PClO_4$: Evidence for a Nodeless Gap" Physical Review Letters **79** 2125 (1997)
5. N. Butch, M. Andrade, and M. Maple, "Resource Letter Scy-3: Superconductivity," American Journal of Physics **76**, 106 – 118 (February 2008)
6. P. Dhakal, G. McMahon, L. Norris, J. Oh, and M. Naughton, "FIB deposited carbon-based superconducting nanowires with Tc ~ 7K" Materials Research Society Symposium Proc. 1206, M16-09 (2009)
7. D. Griffiths, *Introduction to Electrodynamics*, 3rd Ed. (Prentice Hall, 1999)
8. H. Ha, J. Oh, J. Moser, and M. Naughton, "Zero bias conductance peak in an SNS weak link bicrystal of the triplet superconductor $(TMTSF)_2ClO_4$," Synthetic Metals **137**, 1215-1216 (2003)
9. E. Hill, *Communications* University of Redlands (2010)
10. J. Hook, H. Hall, *Solid State Physics*, 2nd Ed. (John Wiley & Sons, Inc., 1991)
11. T. Ishiguro and K. Yamaji *Organic Superconductors with 189 Figures* (Springer-verlag, 1990)

12. I. Lee, M. Naughton, G. Danner, P. Chaikin "Anisotropy Of The Upper Critical Field of $(TMTSF)_2ClO_4$" Physical Review Letters **78**, 3555 (1997)
13. I. Lee, P. Chaikin, M. Naughton, "Exceeding the Pauli Paramagnetic Limit in the Critical Field of $(TMTSF)_2PF_6$" Physical Review B **62** 22 (2000)
14. I. Lee, S. Brown, W. Clark, M. Strouse, M. Naughton, W. Kang, P. Chaikin, "Triplet Superconductivity in an Organic Superconductor Probed by NMR Knight Shift" Physical Review Letters **88** 017004 (2002)
15. E. Lynton, *Superconductivity*, 1st Ed. (Spottiswoode, Ballantyne & Co. Ltd., 1962)
16. G. Rindorf, H. Soling, N. Thorup, "The Structures of Di(2,3,6,7-tetramethyl-1,4,5,8-tetraselenafulvalenium) Perrhenate $(TMTSF)_2ReO_4$ and Perchlorate, $(TMTSF)_2ClO_4$" Acta Crystals **B 38** 2805-2808 (1982).
17. D. Shoenberg, *Superconductivity*, 2nd Ed. (University Press, Cambridge, 1952)
18. S. Thornton and A. Rex, *Modern Physics for Scientists and Engineers* 2nd Ed. (Saunders College Publishing, 1993)
19. I. Utke, P. Hoffmann, J. Melngailis, "Gas-assisted focused electron beam and ion beam processing and fabrication" Journal of Vacuum Science and Technology **B 26(4)** 1197 – 1276 (2008)
20. C. Vaccarella, R. Duncan, C. Sa de Melo, "Triplet superconductors: Josephson effect in quasi-one-dimensional systems" Physica C 391 (2003).
21. W. Zhang and C. Sa de Melo, "Triplet versus singlet superconductivity in quasi-one-dimensional conductors" Advances in Physics **56** 4 (2007)